applied sciences

Article

Mine-Microseismic-Signal Recognition Based on LMD–PNN Method

Qiang Li [1], Yingchun Li [2,*] and Qingyuan He [3]

[1] Shaanxi Yanchang Petroleum (Group) Co., Ltd., Xi'an 710065, China; muzugonsui@163.com
[2] State Key Laboratory of Coastal and Offshore Engineering, Dalian University of Technology, Dalian 116024, China
[3] State Key Laboratory of Coal Resources and Safe Mining, China University of Mining and Technology, Xuzhou 221116, China; 5783@cumt.edu.cn
* Correspondence: yingchun_li@dlut.edu.cn

Abstract: The effective recognition of microseismic signal is related to the accuracy of mine-dynamic-disaster precursor-information processing, which is a difficult method of microseismic-data processing. A mine-microseismic-signal-identification method based on LMD energy entropy and the probabilistic neural network (PNN) is proposed. First, the Local-Mean-Decomposition (LMD) method is used to decompose the mine microseismic signal. Considering the problem of vector redundancy, combined with the correlation-coefficient method, the energy entropy of the effective product-function component (PF) is extracted as the feature vector of mine-microseismic-signal classification. Furthermore, the probabilistic neural network (PNN) is used for learning and training, and the blasting-vibration signal and the coal–rock-mass-rupture signal are effectively identified. The test results show that the recognition accuracy of the PNN is up to 90%, the calculation time and classification effect of the PNN are better, and the recognition accuracy is increased by 15% and 7.5%, respectively, compared with the traditional PBNN and GRNN. This method can accurately and effectively identify the microseismic signals of mines and has good generalization performance.

Keywords: microseismic-signal recognition; local mean decomposition (LMD); energy entropy; probabilistic neural network (PNN); correlation analysis

Citation: Li, Q.; Li, Y.; He, Q. Mine-Microseismic-Signal Recognition Based on LMD–PNN Method. *Appl. Sci.* **2022**, *12*, 5509. https://doi.org/10.3390/app12115509

Academic Editor: Amadeo Benavent-Climent

Received: 23 April 2022
Accepted: 24 May 2022
Published: 29 May 2022

1. Introduction

As a currently more advanced and effective ground-pressure-monitoring technology, microseismic monitoring is increasingly used in the mining field [1–3]. Microseismic monitoring mainly uses waveform analysis of vibration signals to obtain time, space and intensity information of microseismic events [4]. However, the signals collected by the sensor are mixed with interference signals such as blasting and mechanical noise. The blasting-vibration signal is the most difficult to identify because its time-frequency characteristics are closest to the coal-and-rock-mass-fracture signal. At present, this problem mainly depends on manual identification. Affected by individual factors, there may be misjudgment, which greatly affects the accuracy of mine-microseismic-information processing [5–7]. Therefore, how to extract effective coal-and-rock-mass-rupture signals from many waveform signals for mine-dynamic-disaster prediction is particularly important [8].

Time-frequency analysis is one of the main methods to identify microseismic-signal waveforms in micro-mines. For the effective identification of coal-and-rock-mass-rupture signals and blasting-vibration signals, scholars at home and abroad have carried out extensive research on time-frequency analysis [9]. Zhang et al [10] extracted the characteristics of microseismic signals by the EEMD–SVD method and identified the types of microseismic signals by the ELM algorithm, and obtained a high accuracy rate. Chen et al. [11] adopted a mine-microseismic-event-identification method combining improved wavelet decomposition and an extreme learning machine (ELM). Zhao et al. [12,13] used EMD to recombine the microseismic signal to find its fractal dimension, and constructed the Fisher method with the slope value of the peak starting-up trend line as the feature vector for signal recognition. Vallejos and Mckinnon [14] established a high-precision microseismic-event-identification model based on source parameters through logistic regression and a neural network. Pu et al. [15] studied the performance of ten commonly used machine-learning models for microseismic/blasting-event recognition. Although the above methods are widely used in the field of microseismic monitoring and have achieved significant results, they also have some shortcomings. The Fourier transform is generally not suitable for processing microseismic signals with non-stationary characteristics. Traditional EMD lacks a strong theoretical basis and is prone to modal aliasing and the end effect in the process of signal decomposition. There is a misjudgment phenomenon in the process of selecting effective IMF components based on experience. Wavelet analysis and wavelet packet decomposition have poor adaptive decomposition performance [16]. The Local Mean Decomposition (LMD) method mainly implements signal-adaptive time-frequency analysis through an iterative process [17], and has many applications in fault detection, non-stationary-signal analysis [18], and seismic-signal recognition [19]. Tao et al. [20] proposed a novel Adaptive Complementary Ensemble Local Mean Decomposition (ACELMD) for complex underwater acoustic signals. Through simulation tests, they found that this method reduces modal aliasing. Zhao et al. [21] used a compound interpolation envelope (CIE) LMD method to evaluate the local non-stationary characteristics of mechanical vibration signals. The relevant literature shows that the LMD method overcomes the problem of EMD mode aliasing, and has great advantages in suppressing the end effect and processing non-stationary signals [22].

The probabilistic neural network (PNN) is a feedforward neural network implemented by Bayesian strategy, which is suitable for pattern-recognition applications. For example, Li et al. [23] used a probabilistic neural network (PNN) to improve the accuracy of seabed-sediment identification. Chaki et al. [24] classified lithology from multiple seismic attributes based on a probabilistic neural network (PNN) and obtained high accuracy. In the pattern classification, compared with the traditional neural-network structure, the probabilistic neural network (PNN) shows the advantages of short learning time and high accuracy.

In view of this, this paper proposes an LMD–PNN model that combines the local-mean-decomposition energy entropy and a probabilistic neural network to identify microseismic signals in mines. LMD is used to decompose the coal-and-rock-mass-fracture and blasting-vibration signals, and the optimal product-function (PF) component is selected by correlation analysis. Then, the feature vector is constructed and combined with the LMD energy entropy. Finally, the PNN method is used to realize the automatic identification of microseismic signals.

2. Basic Theory

2.1. Local Mean Decomposition (LMD)

As a signal-adaptive time-frequency-processing method realized through an iterative process [16], local mean decomposition (LMD) constructs the local mean and local envelope function of the signal, and separates it into the multiplication product of the envelope signal representing instantaneous amplitude and pure frequency-modulation signal, and then obtains a series of product-function (PF) components [22]. The local mean decomposition of the original signal can reduce the interference signal and obtain a more effective real signal.

The main calculation flow of LMD is as follows. First, we should find the extreme value of signal $x(t)$ and calculate the local mean and local envelope function by moving average. Then, the local mean function is separated and the residual signal is demodulated by pure frequency-modulation. We should accumulate all local envelope functions $a_p(t)$ and the first pure frequency-modulation signal $s_p(t)$ to obtain the first PF component $F_{PFp}(t)$, as shown in Equation (1). Finally, the residual signal $u_k(t)$ is decomposed. The above steps need to be calculated iteratively, so as to convert the original signal into n PF components and one residual component $u_k(t)$, as expressed in Equation (2).

$$F_{PFp}(t) = a_p(t)s_p(t) \tag{1}$$

$$x(t) = \sum_{p=1}^{n} F_{PFp}(t) + u_k \tag{2}$$

2.2. Energy Entropy

Energy entropy has a strong negative correlation with the regularity of time series and is generally used to measure the regularity of time-series signals [25]. The energy-distribution changes of mine microseismic signals are closely related to signal types with different frequency characteristics. Energy entropy can effectively express the energy-distribution characteristics of vibration signals in the time-frequency domain, so the LMD energy entropy can be used as a feature vector.

The LMD energy entropy describes the time-frequency energy change of the signal by halving the time envelope characteristics of the product-function (*PF*) component, and the envelope energy $E(p)$ is calculated by Equation (3).

$$E(p) = \int_{T_p} a_p(t)^2 dt = \int_0^{\infty} a_p(t)^2 dt = \sum_{i=1}^{m} a_p(i)^2 \tag{3}$$

where $a_p(t)$ is the envelope of the PF component of the p-th product function, $a_p(t)$ is the i-th discrete data of $a_p(t)$, m is the number of discrete data of $a_p(t)$. $i = 1, 2, \cdots, m$, and Tp is the time range of the p-th PF component. The envelope signal energy of the PF component of the product function is normalized, and the proportion $e(p)$ of the p-th characteristic PF component in the total energy is calculated, as shown in Equation (4).

$$e(p) = \frac{E(p)}{\sum\limits_{p=1}^{n} E(p)} \tag{4}$$

Finally, the energy entropy $H(p)$ of the PF component is determined based on the definition of energy entropy, as shown in Equation (5), so as to characterize the complexity of different types of microseismic signals on a time scale. In the following equation, $H(p)$ is the energy entropy of the p-th PF component.

$$H(p) = -e(p)\lg e(p) \tag{5}$$

2.3. Probabilistic Neural Network (PNN)

The Probabilistic Neural Network (PNN) [26] combines Gaussian probability-density-function estimation and Bayesian optimization rules to complete classification estimation based on probability density. Therefore, the PNN has the following advantages: a simple learning process and fast training speed, more accurate classification and good fault tolerance, etc.

The network topology of the PNN is shown in Figure 1. Its structure mainly includes an input layer, a hidden layer and an output layer. Different from the traditional neural network, the output layer of the PNN uses the competitive output of the probability-estimation method to replace the previous linear output, so as to obtain an effective neuron through the probability, and the output of the neuron is used as the final classification result.

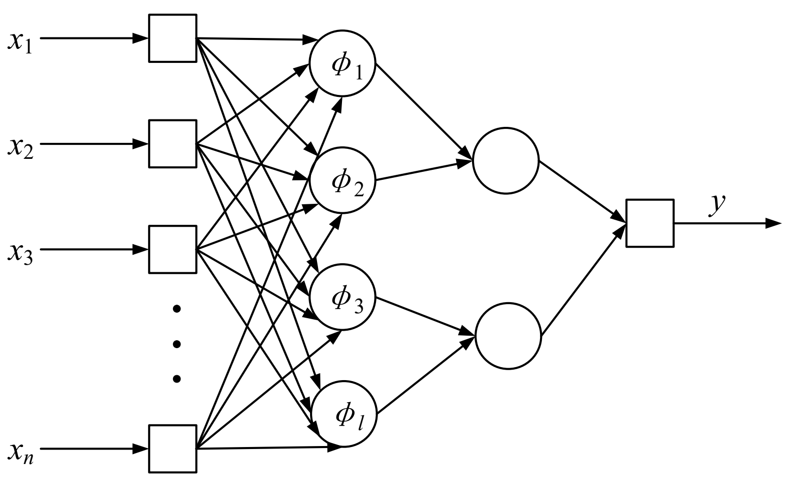

Figure 1. PNN network structure.

The hidden layer and the output layer are connected by a radial basis function which is a Gaussian function, as shown in Equation (6). After the neural-network weights are obtained through training, the final result of the output layer can be obtained.

$$y_k(x,\sigma) = \frac{1}{l_k(2\pi)^{n/2}\sigma^n}\sum_{i=1}^{l_k}\exp(-\sum_{j=1}^{n}\frac{\left(x_{ij}^{(k)} - x_j\right)^2}{2\sigma^2}) \tag{6}$$

Among them, l_k represents the number of k categories; n represents the number of features; σ represents the smoothing parameter, generally between 0 and 1; $x_{ij}^{(k)}$ represents the j-th data in the i-th neuron under the k-th category.

3. LMD–PNN Microseismic-Signal Recognition

3.1. Feature Extraction

Taking into account the vector-redundancy problem of LMD decomposition components, this paper uses the correlation coefficient to judge the selection of an effective PF component and uses Equation (7) to obtain the correlation coefficient between the PF component and the original microseismic signal, and retains the PF component with a larger correlation coefficient.

$$\rho_{PF_k} = \frac{C(PF_k, x(t))}{\sqrt{D(PF_k)}\cdot\sqrt{D(x(t))}} \tag{7}$$

In the formula, PF_k represents the components decomposed by CLD. The $x(t)$ represents the original microseismic signal. $C(PF_k, x(t))$ represents the covariance between the PF component and the original microseismic signal. $D(PF_k)$ represents the variance of the PF component. $D(x(t))$ represents the variance of the original microseismic signal [16]. The boundary PF components are obtained by LMD, the correlation coefficient in information theory is introduced, the IMF components with low correlation coefficients are eliminated to form optimal groups of PF components, and then the optimal PF component of the LMD energy entropy is obtained by Equation (5). Xu et al. [27] concluded from the experiment that the PF component whose correlation coefficient is less than 0.03 should be discarded. Therefore, this paper selects the correlation coefficient threshold of 0.3, that is, the energy entropy of the PF component with a correlation coefficient greater than 0.3 to construct the eigenvectors of the mine-microseismic-signal-classification model.

3.2. Automatic Recognition Process of Microseismic Signal

The process of microseismic-signal-feature extraction and automatic recognition based on the LMD energy entropy and probabilistic neural network (PNN) is shown in Figure 1. The cross-correlation coefficient is used to select the optimal PF component to construct the feature vector, and the PNN model is learned and trained to realize the automatic identification of the microseismic signal. The specific process is as follows (in Figure 2).

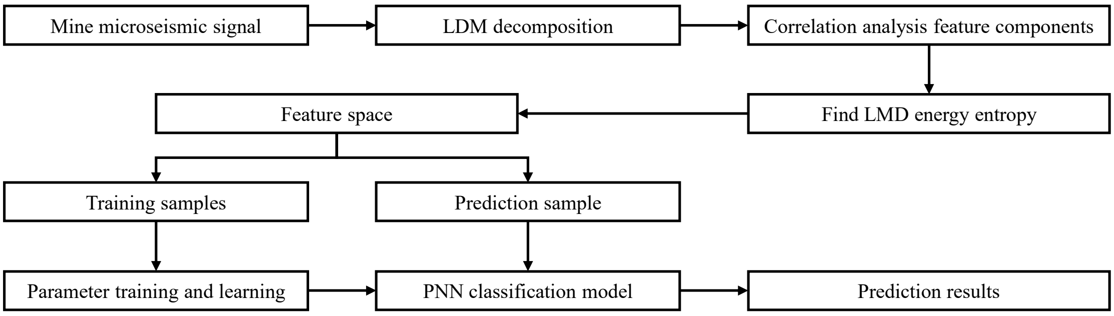

Figure 2. Mine-microseismic-signal-identification process of LMD–PNN.

(1) The vibration signal of the mine site is collected by microseismic equipment, and the collected signal is preprocessed to filter out the noise signal and obtain the mine microseismic signal.
(2) The LMD algorithm is compiled to calculate the mine microseismic signal, and all PF components and residual $u_k(t)$ are obtained by signal decomposition.
(3) Since the extraction of all PF components of the original microseismic signal is likely to cause vector redundancy, which is not conducive to effective classification, the correlation analysis coefficient (Equation (7)) is used to screen the effective PF components.
(4) First, the energy value of the PF component decomposed by the microseismic signal is obtained by Equation (3). Then, the energy value is normalized and substituted into Equation (4). Finally, the LMD-energy-entropy value of the microseismic signal is obtained by Equation (5), and the eigenvector values of all types of mine microseismic signals are obtained.
(5) The PF component entropy with the correlation coefficient greater than 0.3 is taken as the eigenvector value of the mine-microseismic-signal type, and the eigenvector of the PNN mine-microseismic-signal-classification model is constructed.
(6) The random method is used to automatically select the training and prediction samples, the optimal model parameters are automatically obtained by the learning and training system of the samples, and the PNN classification model is established.
(7) Finally, using the established PNN model, the unknown microseismic samples are judged and classified.

4. Simulation-Signal Test

Through the comparative study of simulated signals, the efficiency of the LMD algorithm proposed in this paper is illustrated. The vibration signal $x(t)$ is artificially synthesized by the frequency-modulation signal $f_1(t)$, the amplitude-modulation signal $f_2(t)$ and the sinusoidal signal $f_3(t)$. Considering the noise interference of the mine microseismic signal, white noise $n(t)$ is added to the simulation signal, where the signal–noise ratio is 3 and $t \in [0, 1]$, as shown in Equation (8). The $x(t)$ sampling frequency is 400, and the time-frequency-domain waveform is obtained, as shown in Figure 3. Then, the original vibration signal is decomposed into multiple signal components with different resolutions through LMD and EMD, and then superimposed and compared.

$$\begin{cases} f_1(t) = \sin(100\pi t) \\ f_2(t) = 2.5\cos(40\pi t + \sin(160\pi t)) \\ f_3(t) = 0.8\cos(300\pi t) \\ n(t) = awgn(x, 3) \\ x(t) = f_1(t) + f_2(t) + f_3(t) + n(t) \end{cases} \tag{8}$$

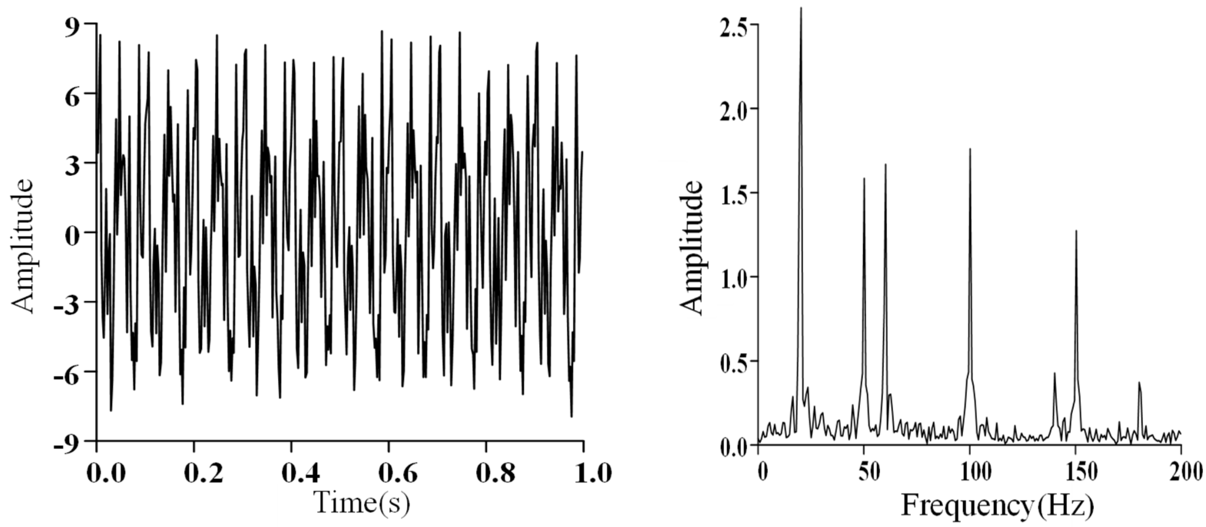

(**a**) (**b**)

Figure 3. Synthetic vibration signal and its frequency spectrum. (**a**) Synthetic vibration signal; (**b**) Synthetic-vibration-signal frequency spectrum.

It can be seen from Figure 3a that the distribution of the synthesized vibration signal in the time domain is disorderly and has no obvious signal-fluctuation characteristics. The synthesized-vibration-signal spectrum has obvious wave fluctuations at 20 Hz, 50 Hz, 60 Hz, 100 Hz and 150 Hz. It shows that the main frequency-band waveforms of this signal are distributed in 20 Hz, 50 Hz, 60 Hz, 100 Hz and 150 Hz. The signal is decomposed by EMD and LMD to obtain the frequency-spectrum diagram of each component, as shown in Figures 4 and 5.

As can be seen from Figure 4, IMF2 obviously exhibits mode aliasing. In addition, multiple low-frequency components originally belonging to the same principal component are obtained. Due to the over-decomposition of the EMD algorithm, too many false modes are generated, which not only delays the calculation time, but also reduces the accuracy of feature extraction. In particular, the fit of IMF3~IMF6 components decomposed by EMD is even more deformed.

It can be seen from Figure 5 that the components PF1 and PF2 obtained by the LMD algorithm correspond to the components above 50 Hz and 25 Hz in the original signal, respectively. Therefore, the decomposition of four components is sufficient to express the lower-frequency signal. It can be seen that the LMD algorithm saves calculation time and feature amounts when extracting microseismic-signal features, which are obvious advantages.

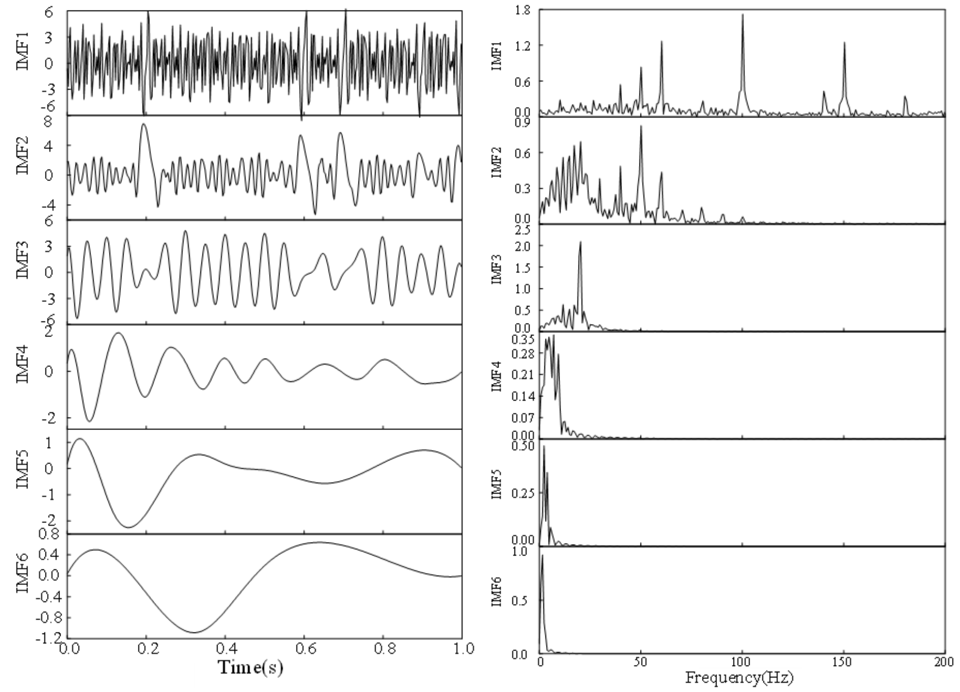

(**a**) (**b**)

Figure 4. EMD decomposition result of the synthesized signal and its frequency spectrum. (**a**) EMD decomposition-component waveform; (**b**) EMD decomposition-component frequency spectrum.

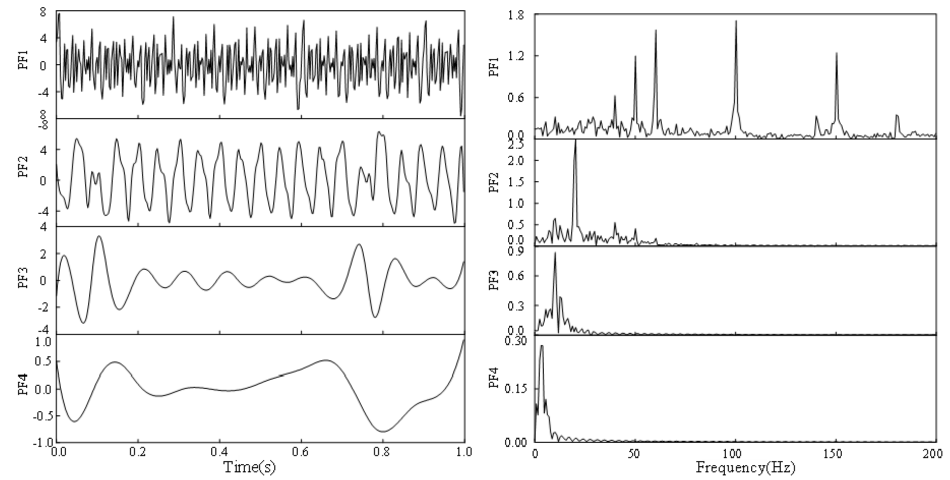

(**a**) (**b**)

Figure 5. LMD decomposition result of the synthesized signal and its frequency spectrum. (**a**) LMD decomposition-component waveform; (**b**) LMD decomposition-component frequency spectrum.

5. Engineering Case Analysis

5.1. Microseismic-Signal-Waveform Analysis

The microseismic-monitoring waveform collected from a coal mine was used for experimental analysis to verify the effectiveness of the method proposed in this article. The mine installed the Canadian ESG microseismic-monitoring system with a sampling rate of 5000 Hz. There are two kinds of microseismic signals that are easy to be confused on site: effective coal-and-rock-mass-fracture events and artificial blasting-vibration events such as construction blasting.

As shown in Figure 6, the system collected two typical coal-and-rock-mass-rupture signals and blasting-vibration signals and their frequency spectra. The obvious difference between the two waveforms is found by comparison. First, the dominant frequency of the coal–rock-fracture-signal waveform is low (below 100 Hz), accompanied by a long duration and slow attenuation rate. Second, the dominant frequency of the blasting-vibration-signal waveform is high (above 100 Hz), accompanied by large amplitude, rapid attenuation rate and short coda. Although these differences can be manually distinguished, it is difficult to automatically identify signals based on the differences. Therefore, the differences between the two signals must be quantified by feature extraction, so as to achieve the purpose of effective automatic recognition.

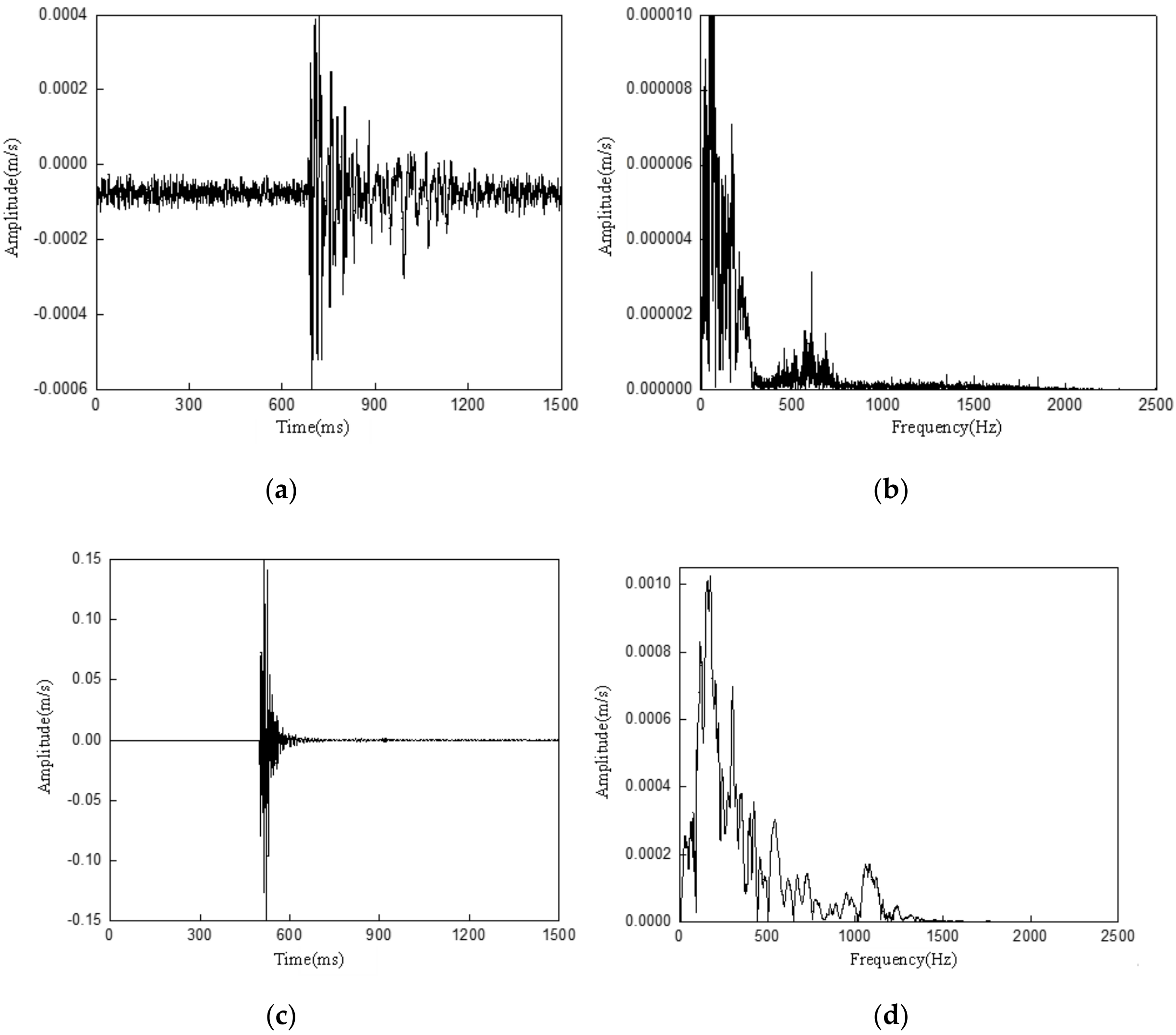

Figure 6. Typical microseismic signals and their frequency spectra in mines. (**a**) Coal-and-rock-mass-rupture signal; (**b**) Coal-and-rock-mass-rupture-signal frequency; (**c**) Blasting-vibration signal; (**d**) Blasting-vibration-signal frequency.

5.2. Feature Extraction

The typical mine coal-and-rock-mass-fracture signal and blasting-vibration signal are decomposed by LMD. The frequency-spectrum results of the microseismic waveform obtained after LMD decomposition are shown in Figure 7. In order to improve the recognition accuracy in the later stage, the decomposed PF components need to be screened to obtain more effective signal features. A group of coal-and-rock-mass-rupture and blasting-vibration signals are randomly selected and calculated using the LMD algorithm, and the correlation coefficient of each PF component is obtained by Equation (7). The results are shown in Table 1. It is clear that the correlation coefficients of the coal-and-rock-mass-fracture signal and the blasting-vibration signal have a relatively consistent change trend, and there is an obvious turning point in PF4. Therefore, we take the correlation coefficient threshold as 0.3, and select PF1~PF4 as the optimal component, and use the LMD energy entropy of PF1~PF4 as the feature vector. As can be seen from Figure 7, the frequency spectrum of PF5 and PF6 components show obvious differences compared with the original signal.

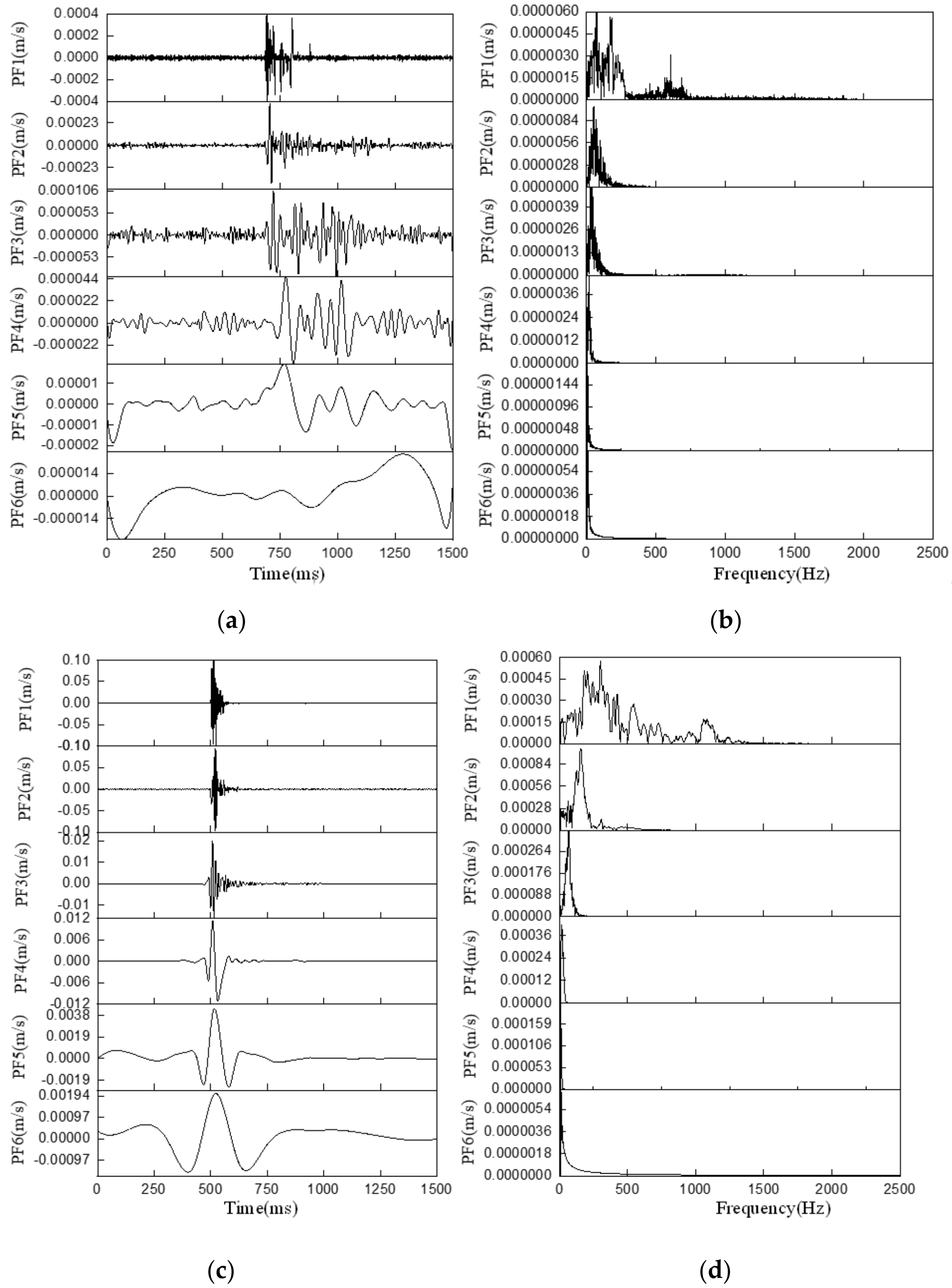

Figure 7. LMD decomposition and frequency spectrum of typical microseismic signals in mines. (**a**) PF component of coal-and-rock-mass-fracture signal; (**b**) PF component frequency spectrum of coal-and-rock-mass-fracture signal; (**c**) PF component of blasting-vibration signal; (**d**) PF component frequency spectrum of blasting-vibration signal.

Table 1. Correlation coefficient of different PF components.

Signal Type	FM1	FM2	FM3	FM4	FM5	FM6
Rupture signal	0.667	0.684	0.305	0.137	0.002	0.001
Blasting signal	0.689	0.761	0.151	0.062	0.011	0.001

The LMD energy entropy of the PF1~PF4 components of a typical mine microseismic signal is shown in Figure 8. It can be seen from the figure that there is a certain regularity in the energy entropy of PF component of microseismic signal at the site. Since the coal-and-rock-mass-fracture signal is mainly concentrated in the low-frequency band, most of the energy entropy of PF3~PF4 is slightly greater than that of PF1~PF2. On the contrary, because the blasting-vibration signal is mainly distributed in the high-frequency band, with high concentration and rapid attenuation, the energy entropy of PF3~PF4 is mostly slightly less than that of PF1~PF2. Therefore, the LMD energy entropy of the PF component can effectively identify mine coal-and-rock-mass-fracture signals and blasting-vibration signals.

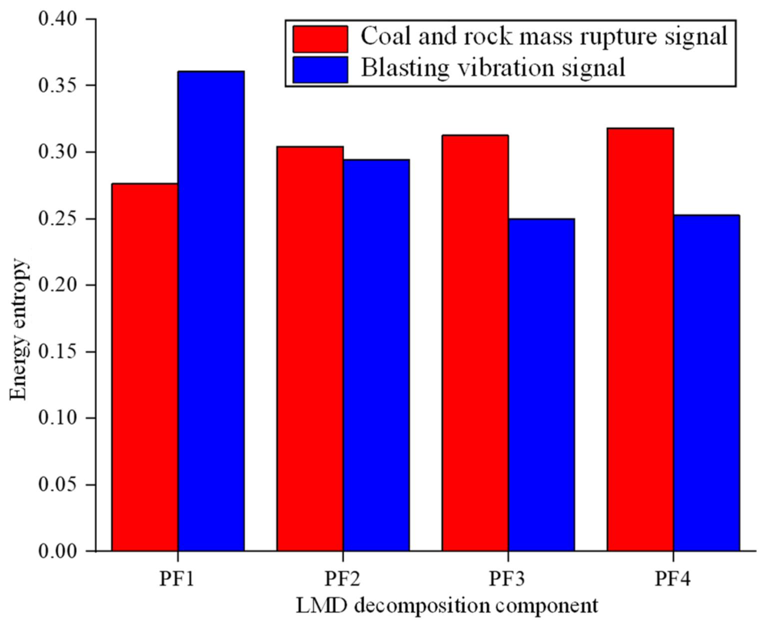

Figure 8. Energy-entropy-comparison diagram of typical microseismic signals in mines.

5.3. PNN Classification and Identification

Using the microseismic data obtained from field detection, 100 groups of coal-and-rock-mass-rupture signals and 100 groups of blasting-vibration signals were randomly selected. The energy entropy of the mine microseismic signal is calculated using the above theory, which is used as the feature vector. From the total sample, 160 groups of training samples and 40 groups of test samples are randomly selected. Assume that the number 1 represents the coal-and-rock-mass rupture signal, and the number 2 represents the blasting-vibration signal. The radial basis function (RBF) is used in the PNN, and its weight and threshold are determined by the learning of training samples without iteration.

In order to verify the effectiveness of the method in this paper, the generalized regression neural network (GRNN), feedforward neural network (BPNN) and PNN are used for comparative experiments. Among them, the hidden-layer node $l = \log_2 n$ of the network structure is selected by the BPNN, where l is the number of hidden-layer nodes, and n is the number of input-layer nodes. The transfer function used in the hidden layer is tan-sigmoid, and the training error and times are set to 0.0001 and 1000, respectively. In the generalized-regression-neural-network (GRNN) model, the accuracy of the data-prediction results depends on the setting of the smoothing factor. The better the set value, the more accurate the data-prediction results. In this paper, the cross-validation method is used to select the smoothing factor, and the training-sample data are randomly divided into 10 sets, 9 of which are used for the training data set, and the remaining 1 data set is used to verify the data set, check the test error corresponding to each value, and search for the output value. The smoothing factor corresponds to the minimum mean square error of the actual values. The four feature vectors are freely combined, and finally 10 types of input vectors are obtained, which illustrate the efficiency of the method in this paper. Model 1 takes FM1 as the input vector. Model 2 takes FM1-FM2 as the input vector. Model 3 takes FM1-FM3 as input vectors. Model 4 takes FM1-FM4 as input vectors. Model 5 takes FM2 as the input vector. Model 6 takes FM2-FM3 as the input vector. Model 7 takes FM2-FM4 as the input vector. Model 8 takes FM3 as the input vector. Model 9 takes FM3-FM4 as the input vector. Model 10 takes FM4 as the input vector. The GRNN and BPNN use the same test set and sample set as the PNN. Figure 9 shows the classification accuracy of the training samples of different models. It can be seen from the figure that the training samples of different models achieved an accuracy rate of more than 90%, and the three methods obtained good learning effects. However, the accuracy difference is more obvious, especially when there is only one feature vector (models 1, 5, 8 and 10), and the training-sample accuracy is the lowest. The fourth group of models has the highest training accuracy, with the BPNN and GRNN all reaching 97%, and the PNN reaching 98%. The method in this paper shows better learning efficiency.

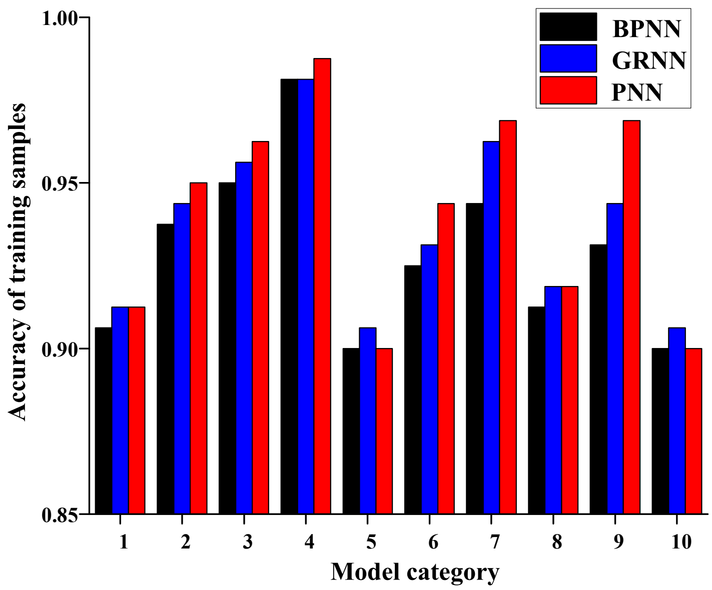

Figure 9. Accuracy comparison of training samples of different input models and different classifiers.

The prediction results of different input models and different classifiers are shown in Figure 10. The PNN classifier proposed in this paper shows better prediction results under different input models compared with the prediction results of the GRNN and BPNN classifiers. Especially when FM1-FM4 are used as input variables, the prediction result of the FNN classifier is the best. Therefore, this paper specifically selects Model 4 with FM1-FM4 as input variables for analysis, and obtains the optimal prediction results calculated by different classifiers, as shown in Table 2. Figure 10 shows the comparison results of the calculation time of different models and different classifiers.

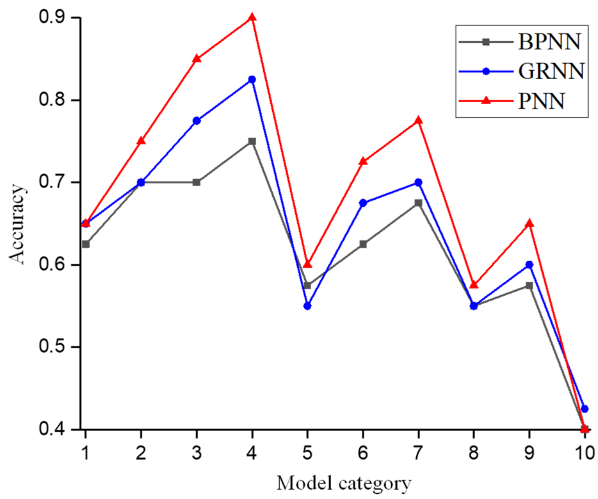

Figure 10. Accuracy comparison of different input models and different classifiers.

Table 2. Comparison of predicted optimal results of different classifiers.

Classification	Blasting Signal (20 Groups)		Rupture Signal (20 Groups)		Total Result (40 Groups)	
	Exact Number	Accuracy	Exact Number	Accuracy	Exact Number	Accuracy
BPNN	16	80.0%	14	70.0%	30	75%
GRNN	17	85.0%	16	80.0%	33	82.5%
PNN	19	95.0%	17	85.0%	36	90%
Total	52	86.7%	47	78.3%	99	82.5%

The classification prediction and recognition results of microseismic signals are shown in Table 2. It can be seen from the classification and prediction results of the three network models that the microseismic-event-classification algorithm based on the PNN has high accuracy, with an average accuracy rate of 90%, which is significantly higher than the accuracy rates of the BPNN at 75% and 82.5%. It can be more effective and accurate in identifying the category of microseismic events. The recognition effect for the blasting-vibration signal is the best. The recognition accuracy of the BPNN is 80.0% for the randomly selected 20 sets of prediction data, and the accuracy rate of the GRNN is improved to 85.0%. The best method in this paper is 95.0%; the correct recognition effect of coal-and-rock-mass-rupture signals is slightly worse than that of blasting-vibration signals. The accuracy rates of the BPNN, GRNN and the method in this paper are 70.0%, 80.0% and 85.0%, respectively. The generalization performance is greatly improved, with obvious recognition advantages. Overall, the average accuracy of the blasting signal of the three methods is 86.7%, which is higher than the 82.5% of the blasting signal of the coal-and-rock mass, and there is still a lot of room for improvement.

In order to evaluate the quality of the PNN, this paper adopts the receiver-operating-characteristic (ROC) indicator, the area-under-curve (AUC) value, and precision. ROC takes the negative–positive rate (false-positive rate, FPR, specificity) as the horizontal axis and the true rate (true-positive rate, TPR, sensitivity) is the curve of the vertical axis, which reflects the sensitivity to the same signal stimulus. The more the curve deviates from the 45-degree diagonal, the more accurate the model classification is. The ROC curves of the three classification models that select the optimal eigenvector model are shown in Figure 11. In Figure 11, we have plotted the average ROC with different colors and bold lines to show the overall performance of the mode (the gray dashed line reflects the ROC of random guessing). From the degree of deviation, it can be seen that the classification accuracy of the PNN is better than the RGNN, and the RGNN is better than the BPNN.

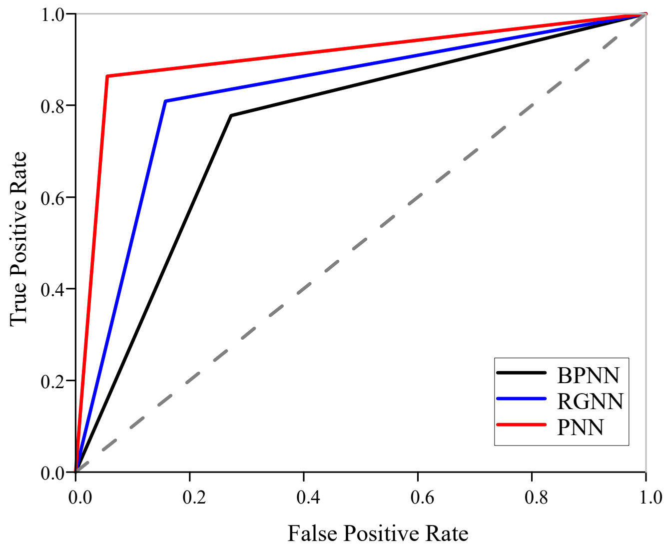

Figure 11. Comparison of ROC curves of different classifiers.

The value of AUC is the area under the ROC curve. Obviously, the value of this area cannot be greater than 1, and the value range is [0.5, 1]. Combined with the ROC curve, the classifier with the larger AUC has the better effect. This value can better reflect the actual classification sensitivity of data. Precision is an evaluation index for prediction results. It represents the percentage of the results predicted by the model as positive samples that are actually positive samples. Figure 12 lists the comparison results of the AUC value and precision of the three methods in this paper. It can be seen that, no matter the precision or the AUC value, the excellence of the classification effect is ranked as PNN, GRNN and BPNN. It can be seen that the PNN in this paper has the best recognition effect for mine microseismic signals.

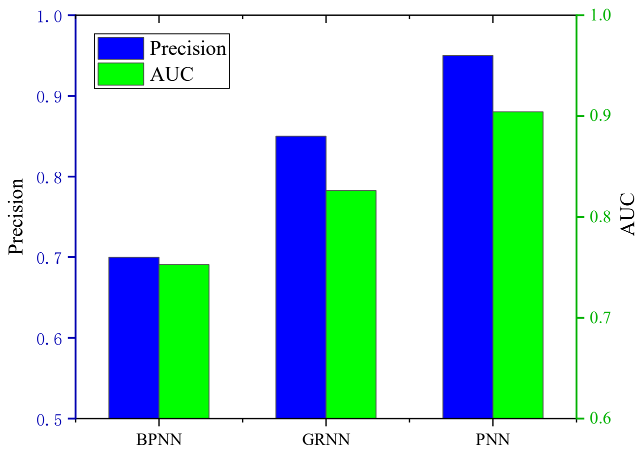

Figure 12. Comparison of ROC and precision of different classifiers.

Figure 13 shows the comparison results of the computation time of different classifiers for different models. It can be seen from Figure 11 that the BPNN model has the longest running time, with an average running time of 0.24 s; the GRNN model has a better running time than the BPNN, with an average running time of 0.23 s; the PNN model has the shortest running time, with an average running time of 0.14 s. The method in this paper shows great advantages in terms of time. Compared with Figure 10, it is found that among the 10 eigenvector models, all three methods show the fourth eigenvector structure (FM1-FM4 as the input vector) with the highest cost performance, that is, the highest accuracy and the shortest running time. Therefore, the energy entropy of PF1-PF4 obtained in this paper with a correlation coefficient threshold of 0.3 is used as a feature vector for automatic identification of PNN microseismic signals, which has the highest accuracy and time efficiency, and has high field-application value.

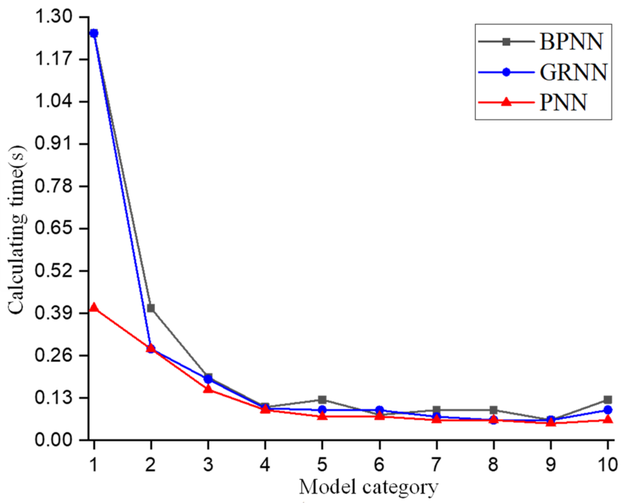

Figure 13. Comparison of calculation time of different input models and different classifiers.

For the engineering site, the initial processing of the data and the later identification and classification are very important. It can be seen from the above analysis that in the identification of microseismic signals, the blasting-vibration signal and the coal–rock-mass-rupture signal are difficult to distinguish due to the similarity of the spectral characteristics. The method in this paper can greatly reduce the workload of manual identification, effectively identify effective microseismic events, and help improve the accuracy of microseismic location and microseismic-magnitude calculation.

6. Conclusions

This paper proposes a mine-microseismic-signal-identification method based on the combination of LMD, energy entropy and PNN. This method is used to identify and verify the types of microseismic-monitoring data in a coal mine, and the conclusions are as follows.

(1) There are regularities in the energy-entropy value of the PF component of the measured field microseismic signal. The rupture signals of coal-and-rock masses are mainly concentrated below 100 Hz, and the energy-entropy values of PF3~PF4 are mostly slightly larger than that of PF1~PF2, while the blasting-vibration signals are mainly concentrated above 100 Hz, which is exactly the opposite of the law of coal-and-rock-mass-rupture signals. The mine-microseismic-signal characteristics constructed by LMD and energy entropy can well characterize the time-frequency law of coal-and-rock-mass-rupture signals and blasting-vibration signals, and can effectively express the change characteristics of mine microseismic signals.

(2) The PNN mine-microseismic-signal-identification method proposed in this paper shows a greater identification advantage compared to the BPNN and GRNN methods in terms of prediction accuracy and calculation time. Therefore, the LMD–PNN model is a new effective method for identifying microseismic signals in mines.

Author Contributions: Conceptualization, Q.L. and Y.L.; methodology, Y.L.; software, Y.L.; validation, Y.L. and Q.H.; formal analysis, Y.L. and Q.H.; investigation, Q.L. and Y.L.; resources, Q.L.; data curation, Q.L. and Y.L.; writing—original draft preparation, Q.L. and Y.L.; writing—review and editing, Y.L. and Q.H.; visualization, Y.L. and Q.H.; supervision, Q.L.; project administration, Q.L.; funding acquisition, Q.L. All authors have read and agreed to the published version of the manuscript.

Funding: This research received no external funding.

Informed Consent Statement: Informed consent was obtained from all subjects involved in the study.

Data Availability Statement: The data presented in this study are available on request from the corresponding author. The data are not publicly available due to privacy concerns.

Acknowledgments: The technical staff of the Shaanxi Yanchang Petroleum (Group) Co., Ltd. are appreciated for their assistance.

Conflicts of Interest: The authors declare they have no conflict of interest to this work.

References

1. Yuan, L. Research progress on risk identification, assessment, monitoring and early warning technologies of typical dynamic hazards in coal mines. *J. China Coal Soc.* **2020**, *45*, 1557–1566.
2. Zhang, C.; Jin, G.H.; Liu, C.; Li, S.G.; Xue, J.H.; Cheng, R.H.; Wang, X.H.; Zeng, X.Z. Prediction of rockbursts in a typical island working face of a coal mine through microseismic monitoring technology. *Tunn. Undergr. Space Technol. Inc. Trenchless Technol. Res.* **2021**, *113*, 103972. [CrossRef]
3. Cao, W.Z.; Durucan, S.; Cai, W.; Shi, J.Q.; Korre, A. A physics-based probabilistic forecasting methodology for hazardous microseismicity associated with longwall coal mining. *Int. J. Coal Geol.* **2020**, *232*, 103627. [CrossRef]
4. Ma, C.C.; Li, T.B.; Zhang, H.; Wang, J.F. An evaluation and early warning method for rockburst based on EMS microseismic source parameters. *Rock Soil Mech.* **2018**, *39*, 765–774.
5. Lin, B.I.; Wei, X.I.E.; Zhao, J.J.; Zhao, H. Automatic classification of multi-channel microseismic waveform based on DCNN-SPP. *J. Appl. Geophys.* **2018**, *159*, 446–452. [CrossRef]
6. Duan, Y.; Shen, Y.R.; Canbulat, I.; Luo, X.; Si, G.Y. Classification of clustered microseismic events in a coal mine using machine learning. *J. Rock Mech. Geotech. Eng.* **2021**, *13*, 1256–1273. [CrossRef]
7. Wilkins, A.H.; Strange, A.; Duan, Y.; Luo, X. Identifying microseismic events in a mining scenario using a convolutional neural network. *Comput. Geosci.* **2020**, *137*, 104418. [CrossRef]
8. Cheng, T.D.; Yi, Q.W.; Wu, Y.W.; Dai, C.C.; Cai, G.P.; Yang, L.R.; Yin, B.Y. Application of improved EWT_MPE model in feature extraction of mine micro-seismic signals. *J. Vib. Shock.* **2021**, *40*, 92–101.
9. Jiang, R.C.; Dai, F.; Liu, Y.; Wei, M.D. An automatic classification method for microseismic events and blasts during rock excavation of underground caverns. *Tunn. Undergr. Space Technol.* **2020**, *101*, 103425. [CrossRef]
10. Zhang, J.Y.; Jiang, R.C.; Li, B.; Xu, N.W. An automatic recognition method of microseismic signals based on EEMD-SVD and ELM. *Comput. Geosci.* **2019**, *133*, 104318. [CrossRef]
11. Chen, Z.; Ding, L.L.; Luo, H.; Song, B.Y.; Zhang, M.; Pan, Y.S. Mine microseismic events classification based on improved wavelet decomposition and ELM. *J. China Coal Soc.* **2020**, *45*, 637–648.
12. Zhao, G.Y.; Deng, Q.L.; Li, X.B.; Dong, L.J.; Chen, G.H.; Zhang, C.X. Recognition of microseismic waveforms based on EMD and morphological fractal dimension. *J. Cent. South Univ. (Sci. Technol.)* **2017**, *48*, 162–167.
13. Zhao, G.Y.; Ma, J.; Dong, L.J.; Li, X.B.; Chen, G.H.; Zhang, C.X. Classification of mine blasts and microseismic events using starting-up features in seismograms. *Trans. Nonferrous Met. Soc. China* **2015**, *25*, 3410–3420. [CrossRef]
14. Vallejos, J.A.; McKinnon, S.D. Logistic regression and neural network classification of seismic records. *Int. J. Rock Mech. Min. Sci.* **2013**, *62*, 86–95. [CrossRef]
15. Pu, Y.Y.; Apel, D.B.; Hall, R. Using machine learning approach for microseismic events recognition in underground excavations: Comparison of ten frequently-used models. *Eng. Geol.* **2020**, *268*, 105519. [CrossRef]
16. Dong, L.J.; Sun, D.Y.; Li, X.B.; Ma, J.; Chen, G.H.; Zhang, C.X. A statistical method to identify blasts and microseismic events and its engineering application. *Chin. J. Rock Mech. Eng.* **2016**, *35*, 1423–1433.
17. Dong, L.L.; Jiang, R.C.; Xu, N.W.; Qian, B. Research on Microseismic Signal Denoising Method Based on LMD-SVD. *Adv. Eng. Sci.* **2019**, *51*, 126–136.
18. Liu, Z.L.; Jin, Y.Q.; Zuo, M.J.; Feng, Z.P. Time-frequency representation based on robust local mean decomposition for multicomponent AM-FM signal analysis. *Mech. Syst. Signal Process.* **2016**, *95*, 468–487. [CrossRef]
19. Zhang, X.B.; Liu, C.; Liu, Y.; Wang, D.; Gou, F.Y. Seismic data time frequency decomposition based on local mean decomposition. *J. Jilin Univ. (Earth Sci. Ed.)* **2017**, *47*, 1562–1571.
20. Lu, T.; Yu, F.Q.H.; Wang, J.R.; Wang, X.Y.; Mudugamuwa, A.; Wang, Y.F.; Han, B.K. Application of adaptive complementary ensemble local mean decomposition in underwater acoustic signal processing. *Appl. Acoust.* **2021**, *178*, 107966. [CrossRef]
21. Zhao, H.Y.; Wang, J.D.; Lee, J.; Ying, L. A compound interpolation envelope local mean decomposition and its application for fault diagnosis of reciprocating compressors. *Mech. Syst. Signal Process.* **2018**, *110*, 273–295.
22. Smith, J.S. The local mean decomposition and its application to EEG perception data. *J. R. Soc. Interface* **2005**, *2*, 443–454. [CrossRef] [PubMed]
23. Sun, C.Y.; Hu, Y.; Shi, P. Probabilistic neural network based seabed sediment recognition method for side-scan sonar imagery. *Sediment. Geol.* **2020**, *410*, 105792. [CrossRef]

24. Chaki, S.; Routray, A.; Mohanty, W.K. A probabilistic neural network (PNN) based framework for lithology classification using seismic attributes. *J. Appl. Geophys.* **2022**, *199*, 104578. [CrossRef]
25. Sun, Y.; Yang, F.; Zheng, J.; Zhang, H.; Xu, M.X. Research on microseismic signal denoising based on variational mode decomposition and wavelet energy entropy. *J. Min. Sci. Technol.* **2019**, *4*, 469–479.
26. Specht, D.F. Probabilistic neural networks. *Neural Netw.* **1990**, *33*, 109–118. [CrossRef]
27. Xu, F.; Liu, Y.F. Feature extraction and classification method of acoustic emission signal based on EMD-SVD. *J. Basic Sci. Eng.* **2014**, *22*, 1238–1247.